SPECTRAL AND TEMPORAL RESPONSE OF UV-PUMPED COLLOIDAL QUANTUM DOTS IN POLYMER, THIN-FILM, AND ADDITIVELY-MANUFACTURED STRUCTURES

1st Lt Michael Sherburne, Dr. Sergei Ivanov, Ms. Shruti Gharde, Ms. Gema Alas, Mr. Arjun Senthil, Mr. Dominic Bosomtwi, Dr. Nathan Withers, Dr. Marek Osiński, Dr. Larry Burggraf, Dr. Thomas Weber, Maj Tod Laurvick, PhD

21 January 2022

Technical Memorandum

AIR FORCE INSTITUTE OF TECHNOLOGY
Graduate School of Engineering and Management (AFIT/EN)
2950 Hobson Way
AIR FORCE EDUCATION TRAINING COMMAND
WPAFB, OH 45433-7765

NOTICE AND SIGNATURE PAGE

Using Government drawings, specifications, or other data included in this document for any purpose other than Government procurement does not in any way obligate the U.S. Government. The fact that the Government formulated or supplied the drawings, specifications, or other data, does not license the holder or any other person or corporation; or convey any rights or permission to manufacture, use, or sell any patented invention that may relate to them.

Qualified requestors may obtain copies of this report from the Defense Technical Information Center (DTIC) (`http://www.dtic.mil`).

AFIT-22-ENG01006 HAS BEEN REVIEWED AND IS APPROVED FOR PUBLICATION IN ACCORDANCE WITH ASSIGNED DISTRIBUTION STATEMENT.

SHERBURNE.MICHAEL.D.1050457466 Digitally signed by SHERBURNE.MICHAEL.D.1050457466 Date: 2022.01.21 13:55:25 -07'00'

1ST LT MICHAEL SHERBURNE
Graduate Student
Department of Electrical and Computer Engineering

CHANDRAHALIM.HENGKY.1540631324 Digitally signed by CHANDRAHALIM.HENGKY.1540631324 Date: 2022.01.21 16:12:14 -05'00'

DR. HENGKY CHANDRAHALIM
Assistant Professor
AFIT/ENG

This report is published in the interest of scientific and technical information exchange, and its publication does not constitute the Government's approval or disapproval of its ideas or findings.

REPORT DOCUMENTATION PAGE

Form Approved

OMB No. 0704-0188

1. REPORT DATE *(DD-MM-YYYY)*
21-01-2022

2. REPORT TYPE
Technical Memorandum

3. DATES COVERED *(From - To)*
07-25-2018 to 12-9-2021

4. TITLE AND SUBTITLE
Spectral and Temporal Response of UV-pumped Colloidal Quantum Dots in Polymer, Thin-Film, and Additively-Manufactured Structures

5a. CONTRACT NUMBER

5b. GRANT NUMBER
NA000103, 89233218CNA000001, N00014-17-1-2975,N00014-19-1-2117, N00014-18-1-2739

5c. PROGRAM ELEMENT NUMBER

6. AUTHOR(S)
Michael Sherburne* Sergei Ivanov** Shruti Gharde*** Gema Alas*** Arjun Senthil*** Dominic Bosomtwi*** Nathan Withers*** Marek Osiński*** Larry Burggraf* Los Alamos National Laboratory Thomas Weber**** Tod Laurvick*

5d. PROJECT NUMBER

5e. TASK NUMBER

5f. WORK UNIT NUMBER

7. PERFORMING ORGANIZATION NAME(S) AND ADDRESS(ES)
Air Force Institute of Technology*
Graduate School of Engineering and Management (AFIT/EN)
2950 Hobson Way
WPAFB, OH 45433-7765

Center for Integrated Nanotechnologies**
P.O. Box 5800, MS-1315
Albuquerque, NM 87185-1315

UNM Center for High Technology Materials***
1313 Goddard SE, MSC04 2710
Albuquerque, NM 87106-4343

Los Alamos National Laboratory****
PO Box 1663, Mail Stop E526
Los Alamos, NM 87545

8. PERFORMING ORGANIZATION REPORT NUMBER
AFIT-22-ENG01006

9. SPONSORING/MONITORING AGENCY NAME(S) AND ADDRESS(ES)
National Nuclear Security Administration
U.S. Department of Energy
1000 Independence Ave., SW
Washington, DC 20585

Office of Naval Research
875 N. Randolph Street
Suite 1425
Arlington, VA, 22203

10. SPONSOR/MONITOR'S ACRONYM(S)
NNSA, ONR

11. SPONSOR/MONITOR'S REPORT NUMBER(S)

12. DISTRIBUTION/AVAILABILITY STATEMENT
Distribution statement A approved for public release; distribution is unlimited. Public Affairs release approval 88ABW-2022-0026. Other requests for this document shall be referred to AFIT/EN, 2950 Hobson Way, WPAFB, OH 45433-7765.

13. SUPPLEMENTARY NOTES

14. ABSTRACT
An interesting question regarding colloidal quantum dots (CQDs) was how do they compare in terms of both their photoluminescence (PL) spectra and UV-Vis PL lifetime decays in various structures? This paper characterized both of these measurements using six commercially available CQD materials, these being: CdS, CdSe, CdSe nanoplatelets (NPLs), CdSe/ZnS, InP/ZnS, CuInS/ZnS. These nanocrystals were tested in the following structures: CQD-loaded polymer matrix, thin-film, and CQDs dispersed within a 3D printed honeycomb structure. Over the course of the experiments the following effects were observed: Charge-transfer (CT), Förster resonance energy transfer (FRET), and thermal oxidation. The time it took for CQD structures to decay from a experimentally derived modeled normalized intensity of 100% to 0.1% from UV-Vis excitation showed that the slowest decaying CQD loading structure was thin-film (12 ns to > 144 ns) while the fastest structure was CQD-loaded polymer matrix (945 ps to 20 ns). The 3D printed structure utilized SU-8-5 photoresist as a capping polymer to contain the CQDs. This resulted in all of the UV-Vis PL decay spectra for each nanocrystal material to become similar in values until the normalized intensity went below 1%. The 100% to 0.1% normalized intensity decay time for the 3D printed structure was from 10 ns to 44 ns. Out of all of the nanomaterials tested under UV excitation, CdS was demonstrated to be the fastest PL decaying CQD with a 100% to 50% normalized intensity decay time as 545 ps when loaded within a polymer matrix.

15. SUBJECT TERMS
characterization; nanoplatelets; nanotechnology; photoluminescence decay; photoluminescence spectra; quantum dots; temporal response

16. SECURITY CLASSIFICATION OF:			17. LIMITATION OF ABSTRACT	18. NUMBER OF PAGES	19a. NAME OF RESPONSIBLE PERSON
a. REPORT	b. ABSTRACT	c. THIS PAGE			1st Lt Michael Sherburne
UNCLASSIFIED	UNCLASSIFIED	UNCLASSIFIED	SAR	32	19b. TELEPHONE NUMBER *(include area code)* 505-846-6659, research@afit.edu

TABLE OF CONTENTS

Section **Page**

LIST OF FIGURES

Figure **Page**

LIST OF TABLES

Table **Page**

1.0 INTRODUCTION

This paper reports preliminary steps towards the creation of novel Colloidal Quantum Dot (CQD)s and Nanoplatelet (NPL)s-based diagnostics. There are several sensing applications utilizing CQDs: radiation, temperature, electromagnetics, strain, up-converting of wavelengths when paired with another material, and many more [3–6]. UV-Vis PL emission spectra and PL lifetime decays can help select a desired CQDs-based material. Six varieties of CQDs and NPLs from a commercially available source have been selected to emit a usable spectra for use with a UV-Vis streak camera's photocathode. A streak camera is one method in measuring light with picoseconds of temporal resolution [1].

The thickness of quantum dot emitting structures matters for sensing applications such as radiation detection [7]. A bulk amount of quantum dots would help for overall system Quantum Efficiency (QE). Thus, there is also interest to look into how both CQDs and NPLs behave in thicker structures. Two ways of stacking the CQDs: impregnated polymer and dispersion into a 3D printed structure are shown in this paper. In addition, a thin-film structure is shown as a comparison. They are other ways to stack CQDs and NPLs, however ease of fabrication led to using these two methods. To the authors' knowledge, there have been no other papers in prior literature that investigated as many commercially available CQDs and NPLs alongside various fabricated structures [1]. This manuscript is intended to assist engineers and researchers in using commercially available quantum dots for future diagnostics.

2.0 THEORY

CQDs ordinarily have structures similar to those represented graphically in Fig. 1a. Every CQD contains a core, the primary compound [8]. In order to both prevent agglomeration of the nanocrystals and ensure compatibility of the nanocrystals into various media, ligands are bonded to the CQD's surface. Ligands are organic polymer chains that help to functionalize the CQDs [9]. The outer layer in Fig. 1a is called the shell. During synthesis of CQDs, defects occur across the surface of the core. To mitigate this issue, a shell compound material (usually ZnS) is applied around the core. The shell fills in core defects and reduces trap states, thus increasing QE [10]. In addition, shells usually promote a Stokes shift (separation of the emission and absorption spectra) [10, 11]. This also helps increase QE as reabsorption of emitted photons may be greatly mitigated or even eliminated. NPLs are a similar nanocrystal technology to CQDs, albeit both their rectangular and thin geometry cause quantum-well-like optoelectronic properties that can result in Giant Oscillator Strength Transition (GOST) and a narrow emission band [12]. NPLs can also have shells, but have been seen to also have a partial covering of their surface known as a crown [13].

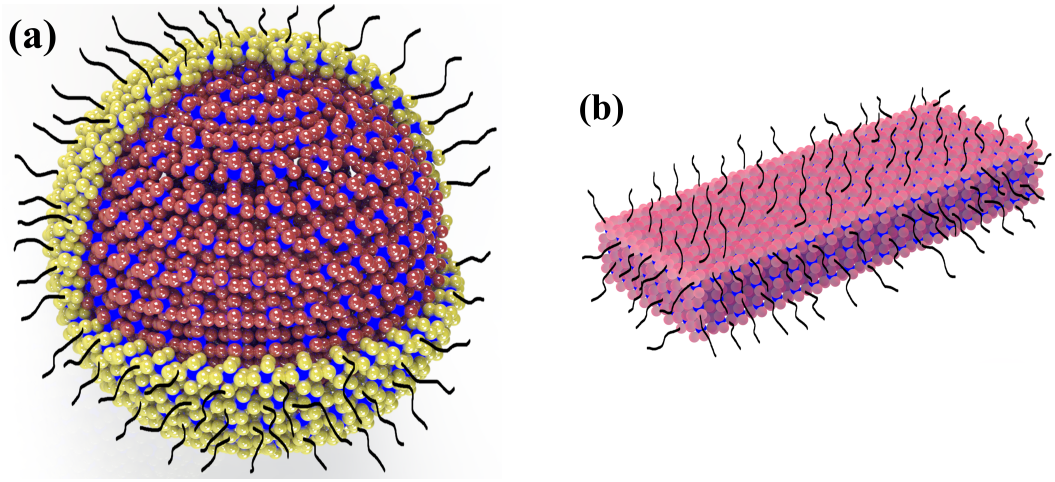

Figure 1. (a) Structures that make up a core-shell CQD. The pink-blue area represents the core, the yellow encompassing the pink-blue area represents the shell, and the black lines represent the ligands. (b) Visual representation of a core-only NPL encapsulated with ligands [1].

The bandgap diagram seen in Fig. 2 visualizes the energy transitions within CQDs, which have discrete energy levels near the band edges. They are confined in a small three dimensional structure whose width of confinement (e.g, spherical CQD diameter) will determine the bandgap energy between the Highest Occupied Molecular Orbital (HOMO) and Lowest Unoccupied Molecular Orbital (LUMO) levels. The HOMO is the highest occupied discrete energy state above the valence band edge and the LUMO is the lowest unoccupied discrete energy state below the conduction band edge. In addition, an excited electron promoted from the valence band to the conduction band will leave a hole and form an exciton (an electron-hole pair that is kept together by Coulomb interaction) [2], [14].

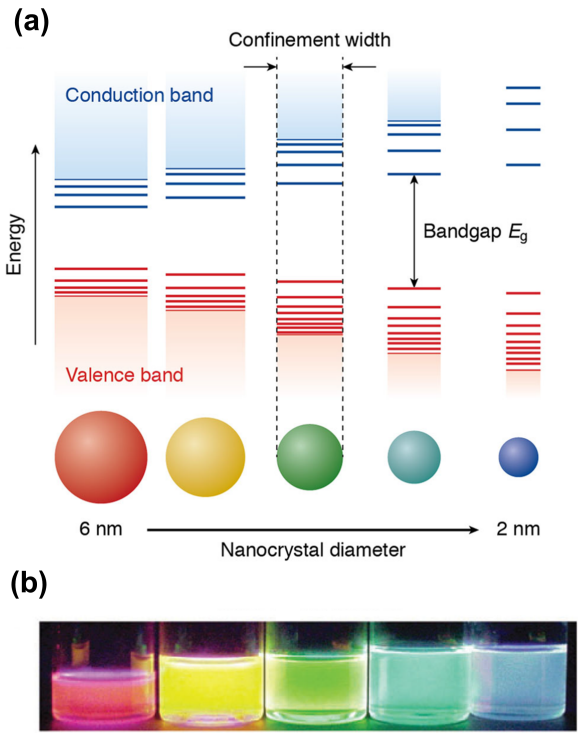

Figure 2. CQD bandgap model with discrete energy levels near the band edges. HOMO band edge is the highest discrete energy state over the valence band edge and LUMO is the lowest discrete energy state under the conduction band edge. (a) CQD emission color represented by a respective bandgap diagram and diameter. (b) Visual representation of CQDs under excitation for each of the CQD diameters represented. Graphic modified from Rabouw *et al.* with written permission for reuse [2].

Photon emission of a CQD occurs when an exciton relaxes back to its ground state (valence band). How fast the emission decays from a CQD is dependent upon radiative recombination mechanism for exciton decay. Simple vertical spin-similar parity-similar core recombination is fastest [15]. For example, additional energy states between the valence band and conduction band levels due to defects in the CQD causes the exciton take a longer decay path [16, 17].

In addition to the explanation of how both CQDs and NPLs emit photons, two spectral phenomena (Förster Resonance Energy Transfer (FRET) and Charge Transfer (CT)) appear in the data. A short introduction of both of these phenomena is explained below.

FRET is a possible inter-nanocrystal interaction within an overall nanocrystal scintillating system. An inter-nanocrystal interaction is where multiple nanocrystals (CQDs) have an effect on each other's emission spectra due to their geometrical proximity. FRET is a process where two compounds/molecules (with one being the donor and the other the acceptor) transfer energy in a non-radiative way. The donor material is excited by incident

energy, but instead of the excited energy within the donor radiatively relaxing, it could transfer over as a phonon to an acceptor material. This phonon between the donor and the acceptor is also known as a virtual phonon. The virtual photon is non-observable and the term is used to help visualize the instantaneous transfer of energy from one fluorophore to another. Possible signs that FRET is occurring would be the observation of a secondary red-shifted peak in the PL spectra and that this red-shifted peak fluoresces later in time than the primary PL emission peak [18]. FRET is a highly distance dependent process and a point dipole-dipole efficiency approximation is given as,

$$E = \frac{1}{1 + (\frac{r}{R_0})^6} \tag{1}$$

where r is the distance between the two fluorophores and R_0 is the Förster distance [19].

In certain circumstances, it is possible for an exciton to transfer charge to a nearby polymer chain (also known as CT) [20]. This is different than FRET which requires a spectral overlap between two fluorophores. However, concepts of FRET are shared with CT such as the proximity of molecules to enhance energy transfer. If a ligand is electron rich, it could transfer its charge from the molecular orbitals to empty or partially filled metal (CQD material) d-orbitals. On the other hand, it is possible to have an electron rich metal having low-lying empty orbitals ligands, which would allow charge to transfer from the metal to the ligand [21], [22].

3.0 APPARATUS AND METHODS

A summary of the nanocrystals bought from NN-Labs can be seen in Table 1. The reason for the various emission wavelengths was due to testing each commercially available material at the lowest emission wavelength as possible. Practically, a lower (bluer) wavelength of emission would mean a higher QE UV-Vis measurement system when measured using a photocathode for a UV-Vis streak camera.

Table 1. Overview of nanomaterials bought from NN-Labs characterized in this paper. *Targeted PL emission at 400 nm, but could be up to 500 nm as stated from NN-Labs.

Material	Geometry	Emission Wavelength (nm)
CdSe	Dot	460
CdSe/ZnS	Dot	520
CdS	Dot	400
CdSe	NPL	400*
$CuInS_2/ZnS$	Dot	530
InP/ZnS	Dot	530

Each nanomaterial was then utilized in the following structures: thin-film, 3D printed, and CQD-loaded polymer which all can be seen in Fig. 3.

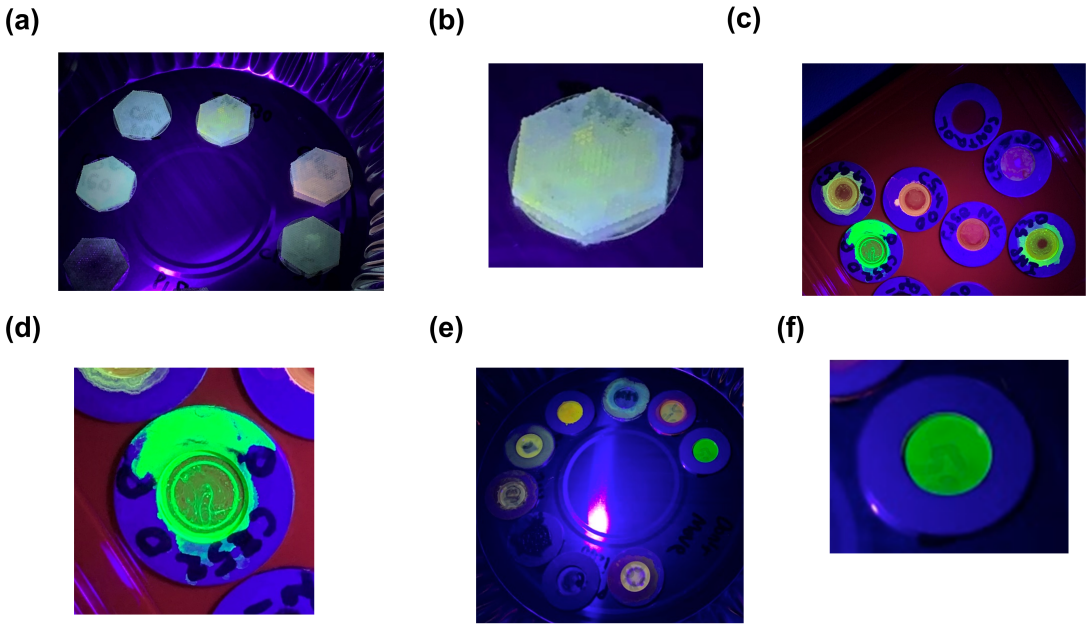

Figure 3. UV excitation of CQDs: (a) dispersed within 3D printed honeycomb structures, (b) magnified view of 3D printed structure, (c) dispersed as a thin-film, (d) magnified view of thin-film structure, (e) loaded within a polymer, and (f) magnified view of polymer structure.

3.1 Thin-Film

CQDs bought as a 10 mg by weight suspended within a toluene solution was dispersed onto the surface of a quartz disc and dried to form a thin-film of the material. A Ultra Violet (UV) excited example of some of the thin-film samples can be seen in Fig. 3c and magnified in Fig. 3d.

The following recipe was used to fabricate each of the thin-film samples: set heat plate to 120℃, place aluminum ring structure onto a small pie tin; using a micropipette, draw out 10µL for CQD solution and 20µL for NPL solution; disperse solution onto the exposed quartz side of the aluminum ring structure; pick up the pie tin and place onto hot plate; let structure bake for ten minutes; pick up the pie tin and place onto aluminum block; and finally allow sample to cool for one minute.

3.2 3D Printed Structure

CQDs bought as described in the previous thin-film section were dispersed within a 3D printed structure, The finished structures can be seen in Fig. 3a and magnified in Fig. 3b.

The following recipe was used to fabricate each of the 3D printed samples: print out 3D printed structure; heat structure in hot oven at 70℃ for 30 minutes on top of a perforated aluminum sheet to remove wax; use boiling water (250℃) to remove remaining supporting wax in 3D print; use pressurized nitrogen gas to dry off the 3D print, submerge 3D print back into boiling water, then quickly drop into a glass jar filled with water to keep it hydrophilic. Once ready to add nanocrystals: drop Isopropyl Alcohol (IPA) onto top of honeycomb structure; disperse CQDs using a micropipette to top of structure; let dry for five minutes; place honeycomb structure on top and center of quartz disc; apply SU-8-5 around circumference of 3D printed honeycomb structure; UV cure for 1000 s; apply SU-8-5 to top of honeycomb structure on top of a spin coater; after UV curing edges, ramp-up speed: 500 RPM, spin speed: 3000 RPM; UV cure for 1000 s; remove excess photoresist on back of quartz disc using acetone, IPA, then water; and finally nitrogen blow dry the sample.

3.3 Polymer Matrix

The CQDs were loaded into a proprietary polymer at a 10% concentration. photo of the cured CQD-loaded polymer under excitation can be seen in Fig. 3e and magnified in Fig. 3f.

The following recipe was used to fabricate each of the CQD-loaded polymer samples: set micropipette to 15 µL, load micropipette and disperse into aluminum disc structure (1.27 cm diameter hole) onto the quartz disc until polymer is level to top of aluminum disc; place structure onto hot plate (set to 120℃) and bake for 20 minutes. Then, place onto an aluminum block and cool for one minute; change temperature of the hot plate to 140℃; place back onto hot plate and bake for 20 minutes; place onto an aluminum block and cool for one minute. Next, change temperature of the hot plate to 180℃; place onto hot plate and bake for 40 minutes; place onto an aluminum block and cool for one minute. Finally, place sample into convection oven (135℃) and let bake for 30 minutes; remove sample from oven and let cool for five minutes.

In this section, both the PL spectra and PL decay data were collected for every nanocrystal sample and structure. The experimental setups were detailed here for the collection of data for each of these characteristics.

3.4 PL Spectra Experiment

The experiments were conducted at approximately room temperature (23℃). A PL spectrofluorometer system (Horiba-Jovin Fluorolog-3) was used and the following settings were: rotation of sample holder was at a right-angle, sample holder angle ($30°$), integration time (0.1 s), wavelength increment (1.00 nm), side entrance slit (1.00 nm), front exit slit (1.00 nm), grating was set to density 1200 $\frac{\text{grooves}}{\text{mm}}$ (Blaze: 500 nm), and averaged scans was set to five. Excitation wavelengths for each nanomaterial were the following: CdSe (335 nm), CdS (320 nm), CdSe NPL (275 nm), CdSe/ZnS (395 nm), $\mathrm{CuInS_2/ZnS}$ (405 nm), InP/ZnS (405 nm), and control (275 nm). All PL intensities collected for the PL spectra experiment were normalized due to the differences in photon counts between different CQDs and the intensity of the excitation lamp was not constant throughout the entire excitation range of the PL spectrometer. This experiment was designed to compare how peaks shifted, widened, or narrowed depending on both the material and structure being used. QE data was not collected due to issues with the hardware.

3.5 UV-Vis PL Temporal Response Experiment

The UV-Vis PL temporal response experiment was conducted at Center for Integrated Nanotechnologies (CINT) within Sandia National Laboratory (SNL). The equipment used was the PTI Felix 32 Spectrofluorimeter and the software used was FeliX Analysis module version 1.2. The available PL decay temporal resolution was ≈ 500 ps. This comes from the Gaussian shape from the excitation diodes that have an $\approx 1.2 - 1.4$ ns Full Width at Half Maximum (FWHM) and the decay measurement begins once the excitation source decays, hence the temporal resolution is about half of the FWHM of the excitation diode pulse. The following excitations wavelengths which were selected to be ≈ 100 nm under the CQD's excitation wavelength were used: 310 nm, 370 nm, and 405 nm. The excitation wavelengths were not collected as the spectrofluorimeter was setup (narrow excitation slit width and wide emission slit width) to collect only the wavelength emission of interest from a given CQD. The software used considered the Instrument Response Function (IRF) when calculating the multicomponent exponential fitting values. The following settings were used for each PL decay spectra: decay was averaged over three times, integration time (0.5 s), and the number of data points was 100. All PL intensities were normalized due to the inherent differences in QE between the different types of nanocrystals and structures. The multicomponent exponential fitting model was used and represented by equation 2.

$$F(t) = F_0 + A_1 \ \exp -\frac{t - t_0}{\tau_1} + A_2 \ \exp -\frac{t - t_0}{\tau_2} + ... \tag{2}$$

From equation 2, F_0 is the initial intensity, $A_{\#\mathrm{s}}$ are the preexponential components, $\tau_{\#\mathrm{s}}$ are the decay constants in ns, t is present time in ns, and t_0 is the initial time in ns. The multicomponent exponential model using anywhere from two to four exponential components is similar to the bi-exponential model which has been determined to make a good approximated fit of a CQD's decay [23].

4.0 RESULTS AND DISCUSSIONS

Both the experimentally collected PL spectra and multicomponent exponential model PL decay data were discussed in this section.

4.1 PL Spectra Experimental Results

PL spectras collected for all three structures: thin-film, 3D printed, and polymer can be seen in Fig. 4. This section went into further detail about notable spectral changes and why these spectral changes occur in each nanomaterial.

4.1.1 CdS PL Spectra

The closest spectra to the manufactured peak PL wavelength (400 nm) was the CQD-loaded polymer matrix. However, the CQD-loaded polymer matrix also emitted a secondary peak at around 530 nm and the same peak also occurred in the thin-film structure. This secondary peak does not align with any of the control peaks. FRET could be ruled out since the CdS CQDs emitting at 530 nm do not overlay between both the donor/acceptor spectras for them to have resonance. This secondary peak most likely occurred from thermal oxidation. This would not be from photo-oxidation since a blue shift of the secondary peak would be expected due to a shrinking CQD core [24]. The secondary peak intensity was the greatest observable change between the CQD-loaded polymer versus that in a thin-film layer. This was due to more CQDs within the CQD-loaded polymer compared to the thin-film and the amount of thermal oxidation was more pronounced during the fabrication process (applied heating) of the CQD-loaded polymer.

A PL emission continuum occurred at lower wavelengths than the main peak PL emission wavelength in the 3D printed structure. Similar to the CdSe/ZnS and InP/ZnS materials, this continuum was most likely due to CT between the CQDs and the surrounding polymer materials. The SU-8-5 photoresist used to cap the CQDs within the 3D structure was the most likely cause of this CT. Comparing the PL emission spectra measured, the reason why the CQD-loaded polymer did not show this continuum trend was likely due to the design of the CQD-loaded polymer to keep charge within the CQDs.

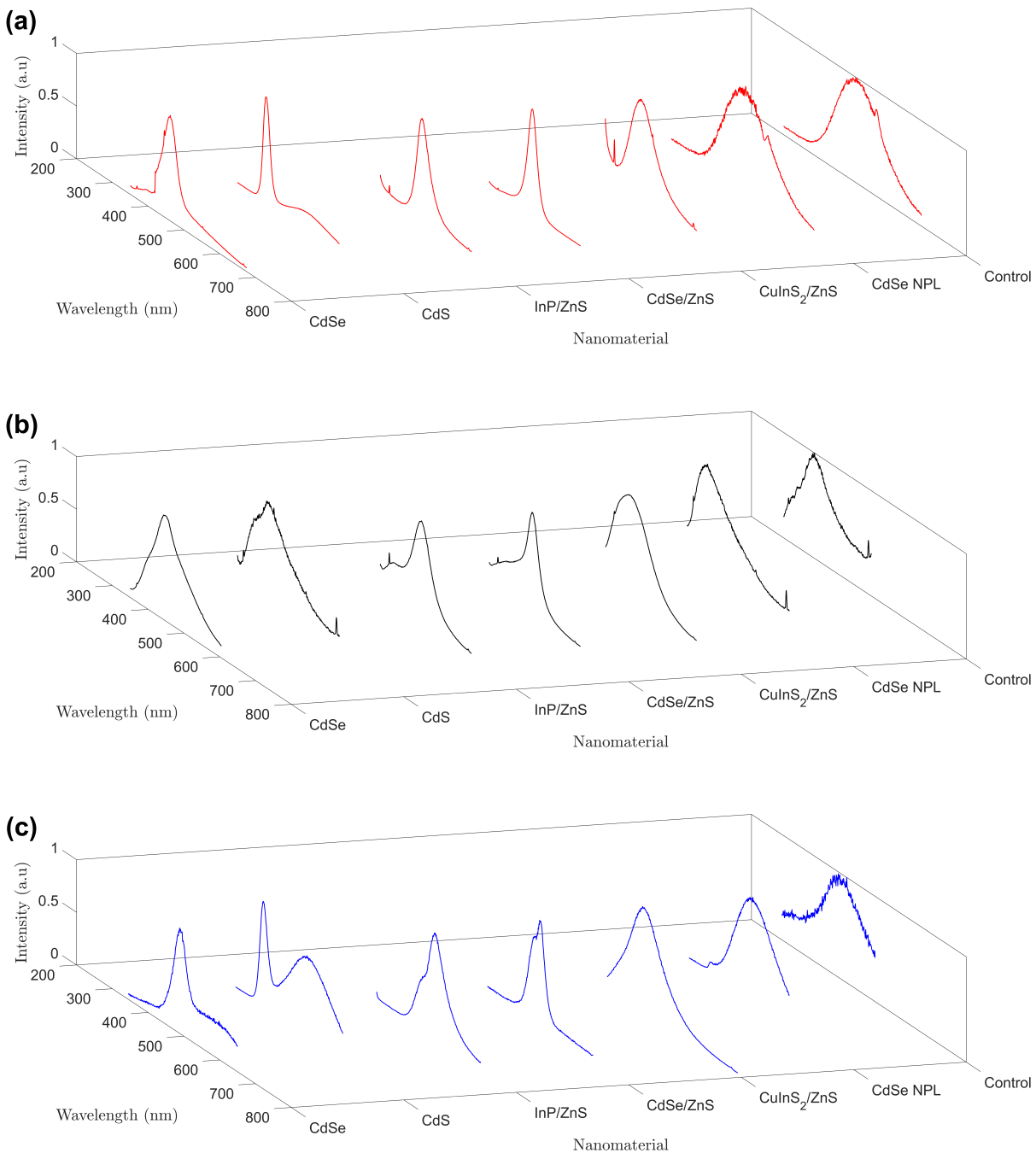

Figure 4. PL spectras of: CdSe, CdS, InP/ZnS, CdSe/ZnS, $CuInS_2$/ZnS, CdSe NPL, and control applied: (a) as a thin-film, (b) into a 3D printed structure, (c) into a polymer structure.

4.1.2 CdSe PL Spectra

These CQDs showed less thermal oxidation indicators than the CdS CQDs. The presumed thermal oxidation peak did start to occur at ≈ 600 nm for the CQD-loaded polymer. The CdSe within the CQD-loaded polymer was red-shifted while the CdSe within the 3D printed structure was blue-shifted. The 3D printed structure showed possible evidence of CT due to the spectral broadening. The thin-film of CdSe was nearly identical to the manufactured PL emission peak wavelength at ≈ 460 nm. However, it also shown a discontinuity at 420 nm. This discontinuity was not due to a faulty measurement due to the sample being averaged five times over. It would be possible for the thin-film of CdSe to oxidize in such a way that the CQDs emitting at ≈ 420 nm were the ones mostly affected. However, with thermal oxidation, it would have been expected to see a red-shifted peak within the thin-film PL spectra. It may also be possible that the ligands surrounding the CdSe when exposed to air could be absorbing or collecting the charge of the CQDs that emit around 420 nm. It would be recommended to fabricate another thin-film CdSe structure to confirm if this discontinuity is a unique physical phenomenon that warrants further investigation or was a structural defect.

4.1.3 CdSe NPL PL Spectra

The NPLs dispersed in the 3D printed structure were the closest to the targeted manufactured peak PL emission wavelength (400 nm). No clearly defined CT peaks occurred for the 3D printed structure, however the spectral broadening could be a possible indicator of CT. The NPLs within the NPL-loaded polymer structure showed a small emission peak at 400 nm, but then the rest of the NPLs heavily red-shifted to ≈ 515 nm.

Evidenced by the NPLs emitting at a low intensity at 400 nm, the NPLs were not stable and heavily thermally oxidized during the fabrication process. Since the NPLs were experimental, manufacturing defects could be the reason, but this could be ruled out since the 3D printed structure showed a clear emission peak at ≈ 400 nm. The red-shifted peak was not material dependent due to the thermal oxidation peaks occurring in the core-only materials. This occurred while hard baking the NPL-loaded polymer up to 180℃ which contributed to a rapid rate of thermal oxidation (especially with no protecting crown material). It would be recommended in the future to hard bake at a lower temperature over a longer period of time. Going over to the thin-film NPL specta, the NPLs emitted at approximately 500 nm. This was expected since this core-only material was prone to thermal oxidation.

4.1.4 CdSe/ZnS PL Spectra

Out of all the materials tested, CdSe/ZnS was the most stable and closest to the manufactured peak PL emission wavelength for all three structures. As seen with the previous materials, a secondary PL peak occurred in the CQD-loaded polymer structure

spectra. This would show more evidence that the fabrication process caused instability to the CQD material. Since a ZnS shell was used, it was unlikely this secondary peak was due to thermal oxidation as the ZnS shell layer was known to prevent or limit thermal oxidation [25]. Instead, FRET could be the reason for this secondary peak. It was observed during the fabrication process that the overall volume of the CQD-loaded polymer shrunk by at least half its original volume. NN-Labs stated this was most likely due to polymer shrinkage which can vary between CQD-loading materials. This would in turn shorten the distance between CQDs and enhance FRET efficiency. The location of the secondary peak would also suggest this was FRET due to both the donor and acceptor spectra overlapping each other. As brought up with the CdS test, the CdSe/ZnS test showed signs of CT with the continuum located on the left slope of the peak PL emission wavelength in the 3D printed structure.

4.1.5 $\mathrm{CuInS_2/ZnS}$ PL Spectra

Out of all the materials tested, $\mathrm{CuInS_2/ZnS}$ showed to have the greatest FWHM. The CQD-loaded polymer structure showed no secondary peak, and was right on the manufactured peak PL wavelength of 530 nm. With no FRET signature present, this would suggest that the CQDs were spaced far enough apart to prevent FRET from occurring. However, CQD-loaded polymer shrinkage was also observed and another reason why FRET was suppressed could be due to the different ligands passivating $\mathrm{CuInS_2/ZnS}$ compared to CdSe/ZnS. The $\mathrm{CuInS_2/ZnS}$ CQDs used a 9:1 mixture of oleic acid and oleyamine. The mixing of two ligands for $\mathrm{CuInS_2/ZnS}$ could have kept the CQDs far enough apart to subdue FRET. The blue-shifted PL emission peak for the 3D printed structure could be attributed to both incompatibility of the ligands with the fabrication process to cause the entire peak to blue-shift and CT of the surrounding SU-8-5 to cause a continuum at lower wavelengths. Despite a relatively wide FWHM, $\mathrm{CuInS_2/ZnS}$ would be the most stable in preventing additional CT peaks, thermal oxidation, and FRET when fabricating all three of the structures.

4.1.6 InP/ZnS PL Spectra

The stability of InP/ZnS was good for both the 3D printed structure and the thin-film structure with a peak PL wavelength at ≈ 530 nm, matching the manufactured peak PL wavelength. There appeared to be a weak 530 nm peak in the CQD-loaded polymer structure, but the majority of the intensity occurred in a secondary peak (≈ 575 nm). Compared to the previous analysis made, CdSe/ZnS showed a similar spectra. With a ZnS shell, thermal oxidation would be highly unlikely. The FRET efficiency was higher in the InP/ZnS sample than the CdSe/ZnS sample due to a higher secondary peak PL emission. From the Leica microscope Z measurements, InP/ZnS was $100\,\mu\mathrm{m}$ thicker than CdSe/ZnS.

The InP/ZnS sample was also jelly-like in consistency versus the more liquid CdSe/ZnS sample. The most feasible hypothesis would be that a thicker CQD-loaded polymer

sample allowed for more emission and re-absorption of the CQD PL emission wavelength, which allowed more photons to enter into CQDs that were experiencing FRET. However, perhaps a more likable scenario would be the percent weight loading. CdSe would be heavier than InP, thus there would have been more InP/ZnS CQDs in a given volume of CQD-loaded polymer material. This increases the likelihood for FRET. A Transmission Electron Microscope (TEM) image would be able to confirm which of these scenarios occurred.

Additionally, the 3D printed structure for InP/ZnS showed a CT peak like CdSe/ZnS, and possibly $\mathrm{CuInS_2/ZnS}$ as well. A slight change in the expected spectral structure of the $\mathrm{CuInS_2/ZnS}$ 3D printed structure showed some evidence of CT at 460 nm. These three separate materials displayed the same CT peak which helped to show that the SU-8-5 photoresist used during the fabrication process of the 3D printed structure was able to emit a significant wavelength intensity with the help of CQDs.

4.1.7 PL Spectra Comparison

Even without QE data, the collected Counts Per Second (CPS) measurements can still be useful when comparing which nanomaterial and structure is the most quantum efficient as a whole. The averaged CPS measurements were taken at the peak emission wavelength. This can be seen in Fig. 5.

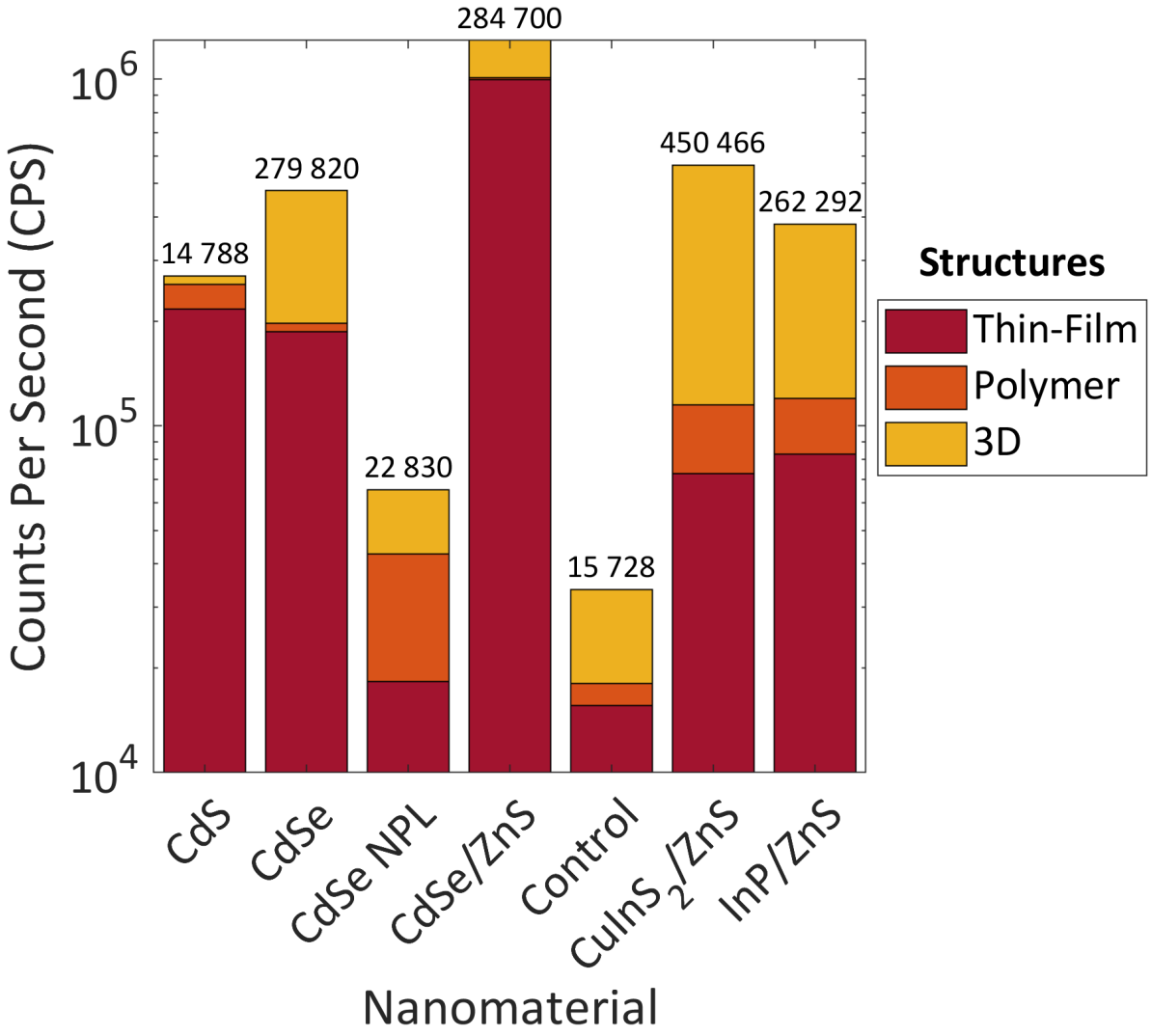

Figure 5. Stacked bar graph comparing the CPS of each nanomaterial with its corresponding structures. The polymer CPS data for CdSe/ZnS is a tiny area in between the 3D printed and thin-film data.

Overall, CdSe/ZnS displayed the highest CPS measurement. In addition, the 3D printed structures showed a higher CPS than the other structures.

4.1.8 Control PL Spectra

The control cases for each of the three structures was able to show what material mechanism of the secondary CT peak occurred in the 3D printed structures. The control polymer case emitted at 466 nm which was about the peak wavelength for where the CT peaks occurred in the 3D printed structures. However, the control 3D printed structure with the SU-8-5 capping layer emitted at 376 nm. This helped to show that CT occurred in

the 3D printed structures since the $460\ nm$ peak only occurred when loaded with CQDs. The control case for the thin-film structure emitted at $495\ nm$. In addition, all three control structures emitted orders of magnitude fewer photons than the structures loaded with CQDs, which helped to confirm that the structures by themselves were not skewing the measurements.

4.2 PL Decay Experimental Results

There were clear differences between the thin-film, 3D printed structure, and polymer CQD samples in terms of their PL decay times. CINT was able to provide all the pre-exponential and decay constant components for use with the multicomponent exponential model in order to plot the PL decays. The values used in the multicomponent exponential models in this paper can be seen in Appendix U. of Ref. [1]. From these values, the PL decay multicomponent exponential curve-fitted models for the thin-film structure were shown in Fig. 6.

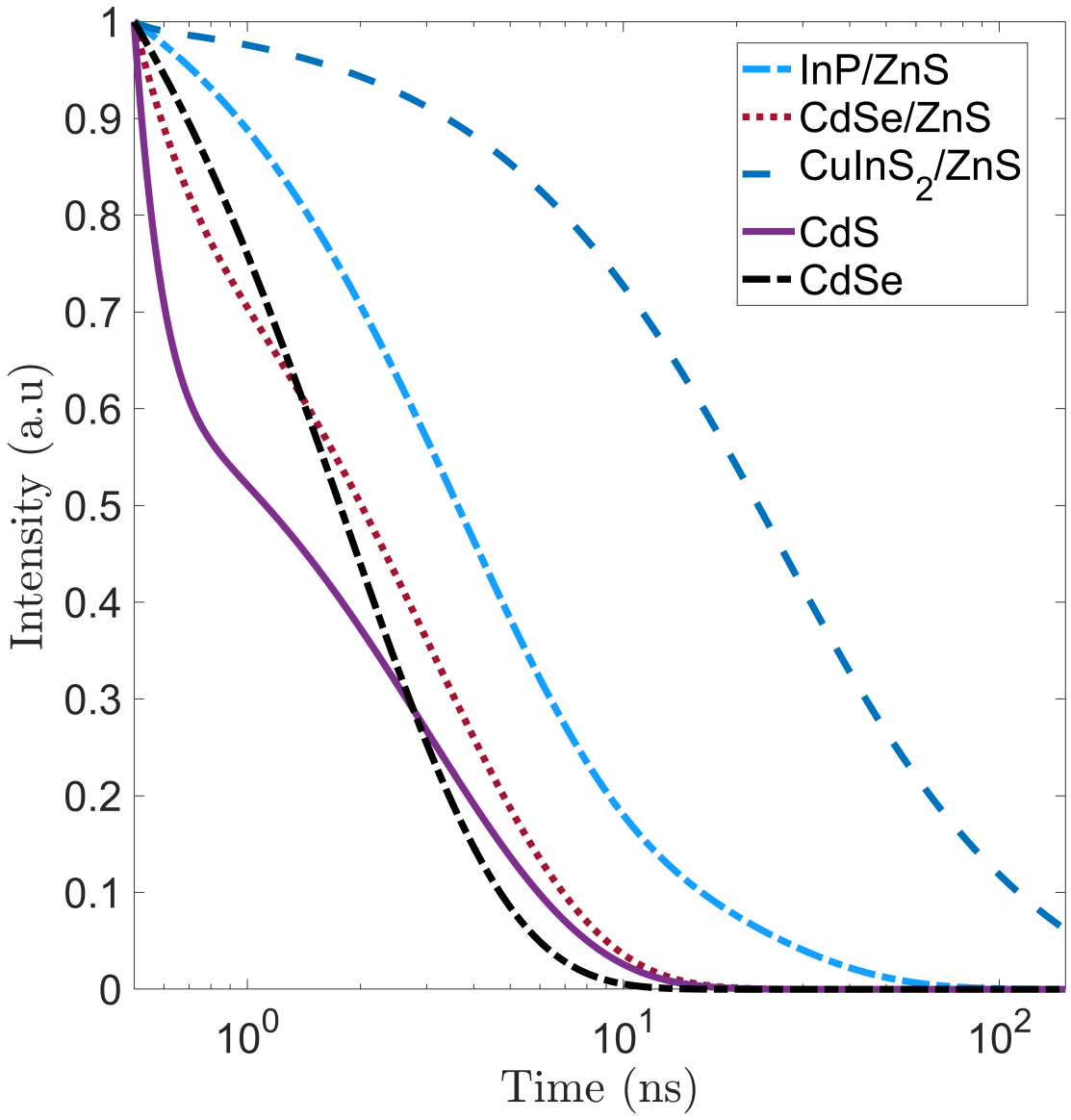

Figure 6. Multicomponent exponential model curve fitting of PL decay of CQDs applied as a thin-film structure. CdSe NPLs were not included due to low QE making UV-Vis PL decay measurements not possible when applied as a thin-film. A control decay was not taken due to the substrate material that is under the thin-film of nanomaterials being quartz which is transparent to UV light.

The fastest decaying CQD applied as a thin-film structure was CdS with a time-to-half-amplitude of 1.13 ns and the shortest overall PL lifetime decay of 13.11 ns to 0.1% of the original normalized intensity was CdSe.

Going over to the next structural case (3D printed structure), the PL decay multicomponent exponential curve-fitted models are seen in Fig. 7.

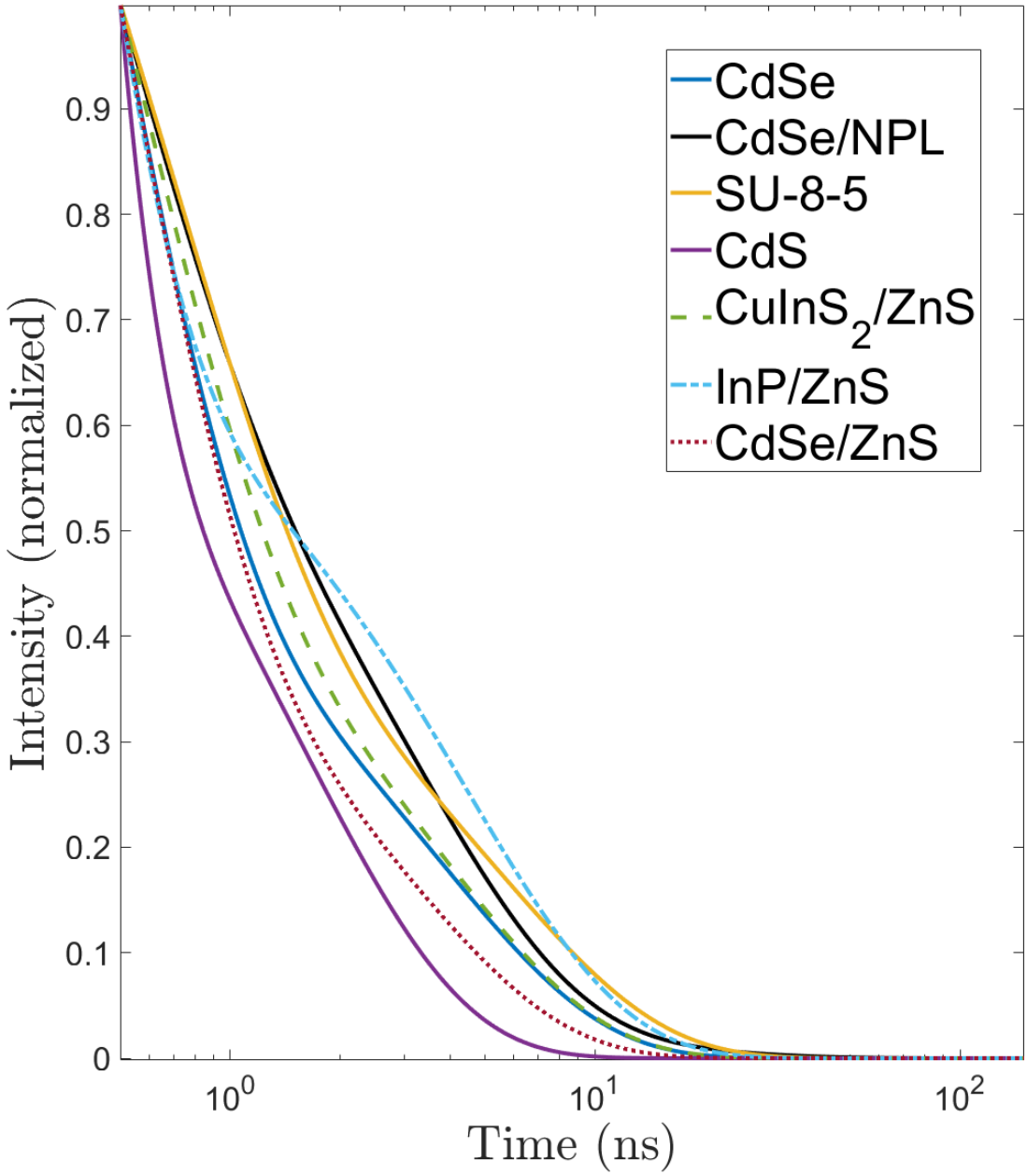

Figure 7. Multicomponent exponential model curve fitting of PL decay of CQDs applied as a 3D printed structure. All samples shown here were loaded with 160 µL **of nanocrystal material within a** 960 µm **thick by** 2.5 cm **diameter 3D printed structure.**

Unlike the thin-film structure, the CQDs dispersed within the 3D printed structure have a closer grouping in terms of their PL decay time. Since CT was noticed on a few of the CQDs, it would be possible that the PL decay for the 3D printed structure was more of a signature of SU-8-5 than the CQDs themselves. However, the 3D printed structure did result in reduction of all of the CQDs to reduce their PL decay time from the thin-film case. The question that needed to be answered was why there was a shift in decay time. Since the shift in decay time was across all of the materials, this was not due to a specific CQD geometric make-up (spherical versus NPL) nor due to the elemental composition of the materials. Hence, the best hypothesis was that this shift was due to CT exciting the faster decaying SU-8-5 polymer molecules. This was most likely not FRET due to no red-shifting of the peaks. The 3D printed structure PL decay results were similar to Au *et al.'s* research due to CT effects [26].

While the presence of CT may not be desirable in terms of overall QE, it happened to be a useful tool to lower PL decay times. As long as the CQD structure was efficient enough to be measurable by a scientific grade camera, CT would help make CQD scintillators more viable in achieving faster temporal resolutions than their bulk counterparts. The main benefit of CT was that the longer phosphorescent emissions appeared to be suppressed. With overall decay times shortened (usually by at least a factor of two), this would help to mitigate the effects of the gating (e.g. pile-up) needed to achieve < 100 ps temporal response measurements. The mechanisms such as CT that caused the fast decay with the 3D printed structure could be used to enhance fast plastic scintillators like Polyvinyl Toluene (PVT) and even integrated with a 3D printed system [27, 28].

Finally, PL decay multicomponent exponential curve-fitted models for the CQD-loaded polymer structure can be seen in Fig. 8.

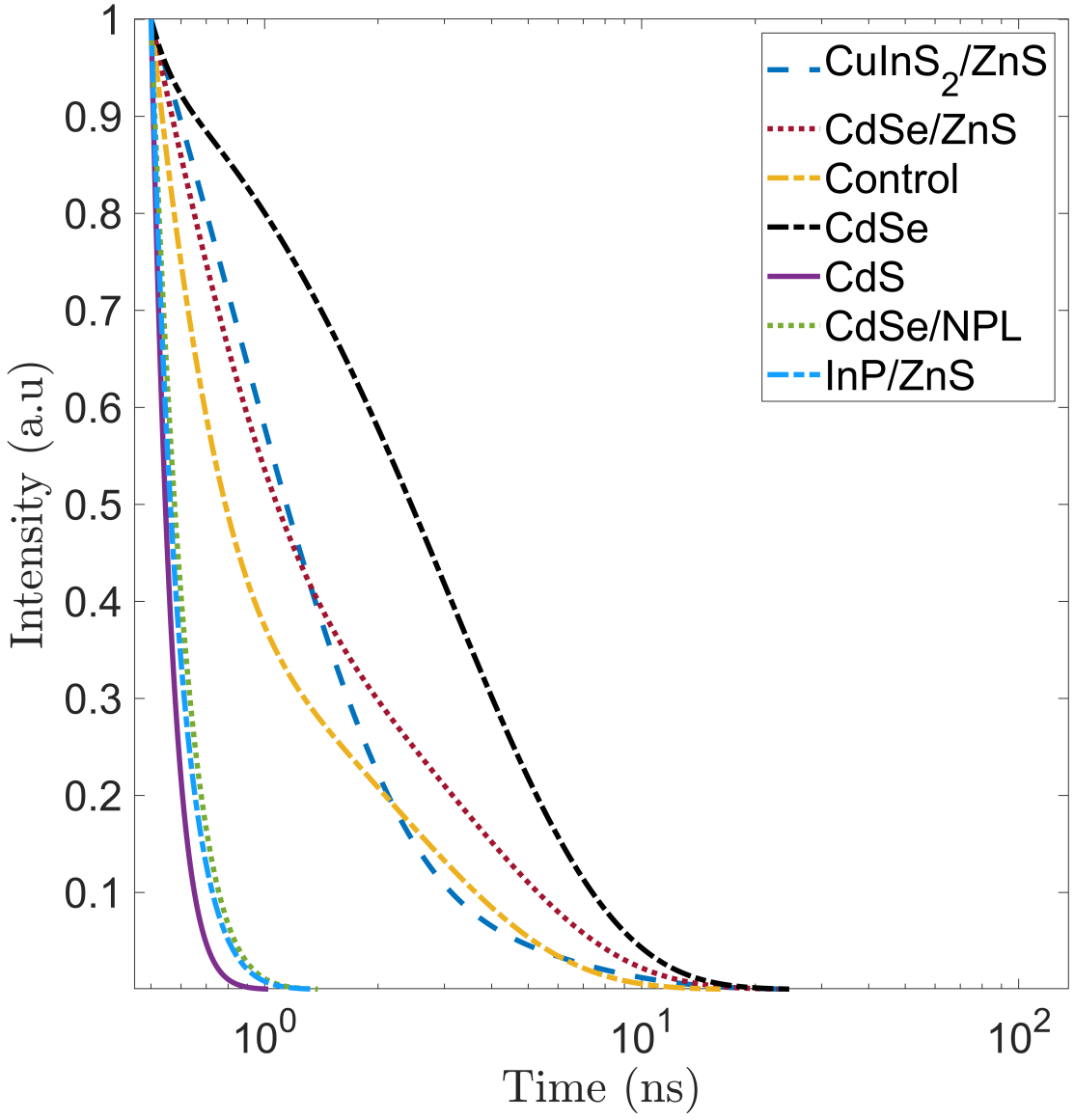

Figure 8. Multicomponent exponential model curve fitting of PL decay of CQDs applied as a CQD-loaded polymer structure. CdSe NPL yielded a non-physical negative value for A_1, its value was set to 0.00, thus this line may not be fully representative of the collected data.

The polymer structure using the proprietary polymer from NN-Labs demonstrated short overall lifetime PL decays with some materials fluorescing < 1 ns. CT was not seen with the polymer samples. However, FRET was seen, which can help lower PL decay time of the emission wavelength of interest. The PL decay curves were not closely grouped like the 3D printed structure, showing support to the hypothesis that the 3D printed structure may have been more of the SU-8-5 PL decay time versus the nanocrystal's actual PL

decay.

4.2.1 Confirmation of FRET Occurrence in InP/ZnS CQD-Loaded Polymer Sample

A PL lifetime decay measurement was taken to confirm that FRET occurred in the double peak seen in both the CdSe/ZnS and InP/ZnS CQD-loaded polymer samples. This measurement for the InP/ZnS sample can be seen in Fig. 9.

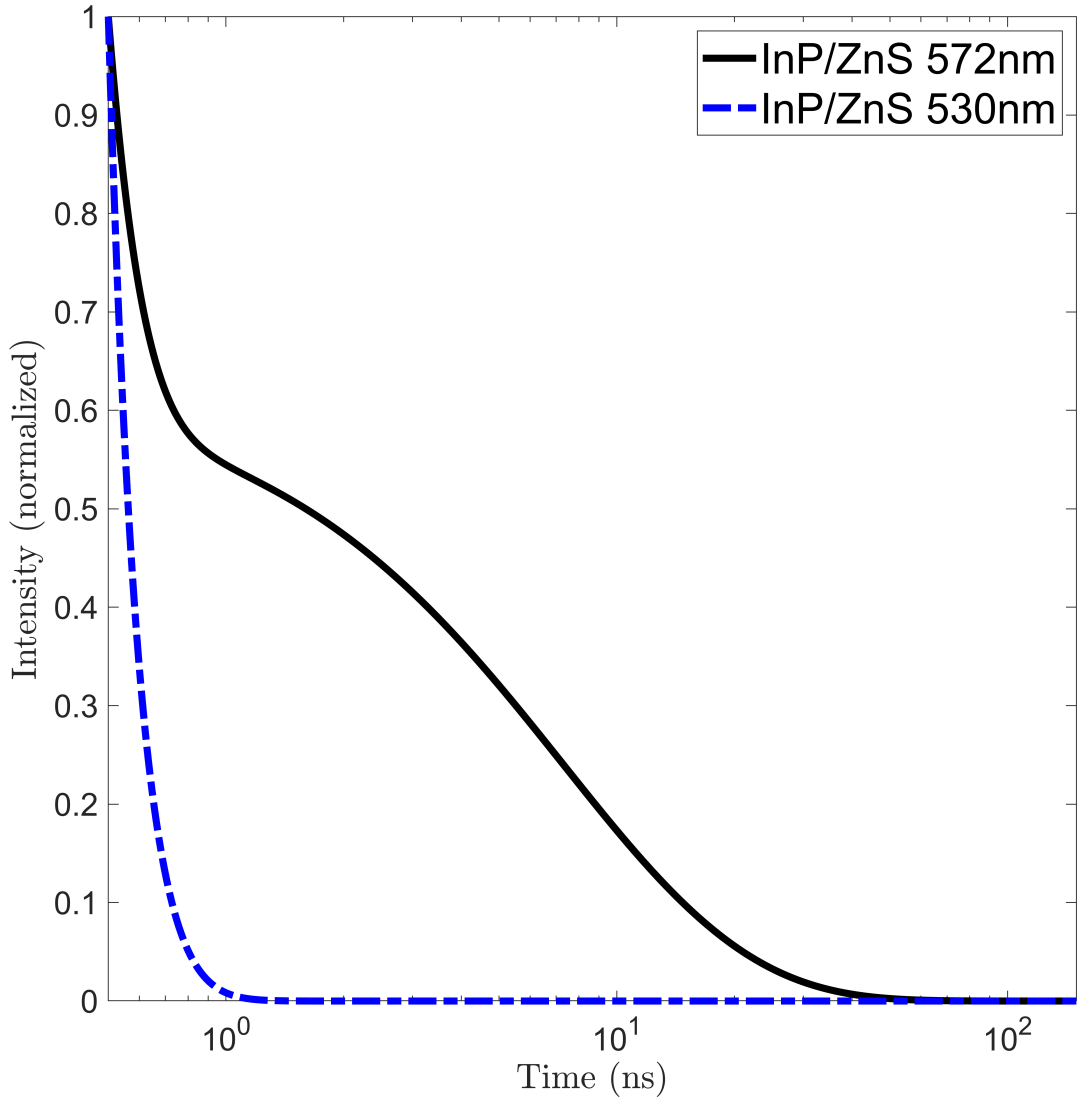

Figure 9. Multicomponent exponential model curve fitting of PL decay of InP/ZnS CQDs applied as a polymer structure. One PL decay line represented the FRET acceptor peak (572 nm) and the other PL decay line represented the donor peak (530 nm).

There was clear evidence of FRET occurring from Fig. 9. The donor emission which was the regular CQD peak emission wavelength (530 nm) quickly decayed in ≈ 1 ns while the acceptor peak (572 nm) was drawn out for ≈ 60 ns. This could be useful for x-ray detection to quickly look at the prompt photon emission of the 530 nm peak while being able to use the acceptor PL decay for energy resolution.

5.0 CONCLUSIONS

Three structures were fabricated and tested using spherical CQDs or NPLs: within a polymer matrix, dispersed into a 3D printed honeycomb structure, and dispersed as a thin-film on top of quartz. The PL spectra for all of the spherical CQDs and NPLs tested showed thermal oxidation degradation peaks for the CQDs without a ZnS shell, FRET for the CQDs with ZnS shells, and CT peaks for the CQDs in the 3D printed structure capped with SU-8-5 photoresist. This CT was especially apparent for both the CdSe/ZnS and InP/ZnS CQDs due to the location of their peak emission wavelength in relation to the CT peak emission wavelength of ≈ 460 nm. This CT peak most likely occurred from the SU-8-5 capping polymer used in the fabrication process.

These changes to the PL spectra such as thermal oxidation, FRET, and CT were important to consider since the stated wavelength of emission for CQDs and NPLs may not be the same as the experimentally measured spectra after being loaded within a structure.

The need to use CQDs as fast x-ray scintillators would encourage future work into utilizing CT effects [29–32]. CQD emission could be up-converted when in the proximity of a polymer designed to take their charge. This could have implications for photonics and improve the QE of CQD and NPL scintillator systems which cannot emit in the blue spectrum. This up-converting property could be useful for defense sensors and technologies such as Night Vision Goggles (NVG)s. In addition, the up-conversion of CQDs using SU-8-5 could be used in Quantum Information Science (QIS) to help tune the CQDs for single photon emission.

ACKNOWLEDGMENTS

This material is declared a work of the U.S. Government and is not subject to copyright protection in the United States. This research was supported in part by the U.S. Dept. of Energy, National Nuclear Security Administration under grant NA000103. This work was supported by the National Nuclear Security Administration of the U.S. Department of Energy under contract 89233218CNA000001. Approved for unlimited release, LA-UR-21-32332. Part of this work was performed at the Center for High Technology Materials, University of New Mexico, under the support of the Office of Naval Research Grants N00014-17-1-2975 and N00014-19-1-2117, and of the Navy HBCU/MI Program Grant N00014-18-1-2739. This work was performed, in part, at the Center for Integrated Nanotechnologies, an Office of Science User Facility operated for the U.S. Department of Energy (DOE) Office of Science. Los Alamos National Laboratory, an affirmative action equal opportunity employer, is managed by Triad National Security, LLC for the U.S. Department of Energy's NNSA, under contract 89233218CNA000001. The views expressed are those of the authors and do not reflect the official policy or position of the U.S. Air Force, Department of Defense, Department of Energy, the U.S. government, or

the University of New Mexico.

6.0 REFERENCES

[1] M. Sherburne, “X-ray detection and strain sensing applications of colloidal quantum dots,” Master’s thesis, Air Force Institute of Technology, Mar. 2020.

[2] F. T. Rabouw and C. de Mello Donega, “Excited-state dynamics in colloidal semiconductor nanocrystals,” *Topics in Current Chemistry*, vol. 374, no. 5, Aug. 2016.

[3] R. Turtos, S. Gundacker, A. Polovitsyn, S. Christodoulou, M. Salomoni, E. Auffray, I. Moreels, P. Lecoq, and J. Grim, “Ultrafast emission from colloidal nanocrystals under pulsed x-ray excitation,” *Journal of Instrumentation*, vol. 11, 2016.

[4] D. Pugh-Thomas, “Luminescent quantum dots for high temperature sensing,” Ph.D. dissertation, University of Virginia, May 2012.

[5] J. Kainz, S. A. Mikhailov, A. Wensauer, and U. RÃ¶ssler, “Quantum dots in high magnetic fields: Calculation of ground-state properties,” *Physical Review B*, vol. 65, no. 11, Feb. 2002.

[6] M. D. Sherburne, C. R. Roberts, J. S. Brewer, T. E. Weber, T. V. Laurvick, and H. Chandrahalim, “Comprehensive optical strain sensing through the use of colloidal quantum dots,” *ACS Applied Materials & Interfaces*, vol. 12, no. 39, pp. 44 156–44 162, Sep. 2020.

[7] N. Tsoulfanidis and S. Landsberger, *Measurement and Detection of Radiation*. Apple Academic Press Inc., 2015, ch. 4, pp. 146–149.

[8] E. O. Chukwuocha, M. C. Onyeaju, and T. S. T. Harry, “Theoretical studies on the effect of confinement on quantum dots using the brus equation,” *World Journal of Condensed Matter Physics*, vol. 02, no. 02, pp. 96–100, 2012.

[9] J. T. W. T. Jie Zhou, Yun Liu, “Surface ligands engineering of semiconductor quantum dots for chemosensory and biological applications,” *Materials Today*, vol. 20, no. 7, Sep. 2017.

[10] G. Schmid, *Nanoparticles : from theory to application*. Weinheim: Wiley-VCH, 2004, ch. 3, pp. 93–95.

[11] X. Li, L. Gu, F. Zong, J. Zhang, and Q. Yang, “Temporal resolution limit estimation of x-ray streak cameras using a CsI photocathode,” *Journal of Applied Physics*, vol. 118, no. 8, 2015.

[12] E. I. Rashba, “Gigantic oscillator strengths inherent in exciton complexes,” in *Springer Tracts in Modern Physics*. Springer Berlin Heidelberg, 1975, pp. 150–170.

[13] R. Turtos, S. Gundacker, S. Omelkov, E. Auffray, and P. Lecoq, “Light yield of scintillating nanocrystals under x-ray and electron excitation,” *Journal of Luminescence*, Nov. 2019.

[14] P. Kathirgamanathan, L. M. Bushby, M. Kumaraverl, S. Ravichandran, and S. Surendrakumar, "Electroluminescent organic and quantum dot LEDs: The state of the art," *Journal of Display Technology*, vol. 11, no. 5, pp. 480–493, May 2015.

[15] M. A. Omary and H. H. Patterson, "Luminescence, theory," in *Encyclopedia of Spectroscopy and Spectrometry*. Elsevier, 2017, pp. 636–653.

[16] G. S. Selopal, H. Zhao, G. Liu, H. Zhang, X. Tong, K. Wang, J. Tang, X. Sun, S. Sun, F. Vidal, Y. Wang, Z. M. Wang, and F. Rosei, "Interfacial engineering in colloidal "giant" quantum dots for high-performance photovoltaics," *Nano Energy*, vol. 55, pp. 377–388, Jan. 2019.

[17] W. K. Bae, L. A. Padilha, Y.-S. Park, H. McDaniel, I. Robel, J. M. Pietryga, and V. I. Klimov, "Controlled alloying of the core–shell interface in CdSe/CdS quantum dots for suppression of auger recombination," *ACS Nano*, vol. 7, no. 4, pp. 3411–3419, Apr. 2013.

[18] D. Andrews, "A unified theory of radiative and radiationless molecular energy transfer," *Chemical Physics*, vol. 135, no. 2, pp. 195–201, Aug. 1989.

[19] F. Schaufele, I. Demarco, and R. N. Day, "FRET imaging in the wide-field microscope," in *Molecular Imaging*. Elsevier, 2005, pp. 72–94.

[20] N. I. Hammer, T. Emrick, and M. D. Barnes, "Quantum dots coordinated with conjugated organic ligands: new nanomaterials with novel photophysics," *Nanoscale Research Letters*, vol. 2, no. 6, pp. 282–290, Jun. 2007.

[21] M. A. Rivera, "Metal to ligand and ligand to metal charge transfer bands," Online, Sep. 2019.

[22] J.-S. Chen, M. Li, and M. Cotlet, "Nanoscale photoinduced charge transfer with individual quantum dots: Tunability through synthesis, interface design, and interaction with charge traps," *ACS Omega*, vol. 4, no. 5, pp. 9102–9112, 2019. [Online]. Available: https://doi.org/10.1021/acsomega.9b00803

[23] J. Alvelid, "Investigation of the photophysical properties of quantum dots for super-resolution imaging," Master's thesis, KTH Royal Institute of Technology, 2016.

[24] W. G. J. H. M. van Sark, P. L. T. M. Frederix, D. J. V. den Heuvel, H. C. Gerritsen, A. A. Bol, J. N. J. van Lingen, C. de Mello Donegá, and A. Meijerink, "Photooxidation and photobleaching of single CdSe/ZnS quantum dots probed by room-temperature time-resolved spectroscopy," *The Journal of Physical Chemistry B*, vol. 105, no. 35, pp. 8281–8284, Sep. 2001.

[25] S. Lee, "Synthesis of optimized inp/zns core/shell nanocrystals and TiO_2 nanotubes for quantum dot sensitized solar cells," Master's thesis, Sogang University, 2002.

[26] T. H. Au, S. Buil, X. Quélin, J.-P. Hermier, and N. D. Lai, "Photostability and long-term preservation of a colloidal semiconductor-based single photon emitter in polymeric photonic structures," *Nanoscale Advances*, vol. 1, no. 8, pp. 3225–3231, 2019.

[27] O. Boyraz, A. Tam, and M. Nilsson, "Plastic scintillator enhancement through quantum dot," in *Hard X-Ray, Gamma-Ray, and Neutron Detector Physics XIX*, M. Fiederle, A. Burger, L. Franks, R. B. James, and S. A. Payne, Eds. SPIE, Aug. 2017.

[28] S. Kim and Y.-H. Seoung, "Fabrication and characterization of 3d printed polyvinyl toluene based plastic scintillator," *Journal of the Korean Physical Society*, vol. 75, no. 12, pp. 953–956, Dec. 2019.

[29] A. Wieczorek, "Development of novel plastic scintillators based on polyvinyltoluene for the hybrid J-PET/MR tomograph," Ph.D. dissertation, Jagiellonian University, 2017.

[30] K. D. Rakes, "Evaluating the response of polyvinyl toluene scintillators used in portal detectors," Master's thesis, Air Force Institute of Technology, Mar. 2008.

[31] A. Tam, O. Boyraz, and M. Nilsson, "Plastic scintillator enhancement through quantum dot," *Hard X-Ray, Gamma-Ray, and Neutron Detector Physics XIX*, Aug. 2017.

[32] J. Park, H. Kim, Y. Hwang, D. Kim, and H. Park, "Scintillation properties of quantum-dot doped styrene based plastic scintillators," *Journal of Luminescence*, vol. 146, pp. 157–161, Feb. 2014.

7.0 LIST OF SYMBOLS, ABBREVIATIONS, AND ACRONYMS

CINT	Center for Integrated Nanotechnologies
CPS	Counts Per Second
CQD	Colloidal Quantum Dot
CT	Charge Transfer
DoE	Design of Experiments
FRET	Förster Resonance Energy Transfer
FWHM	Full Width at Half Maximum
GOST	Giant Oscillator Strength Transition
HOMO	Highest Occupied Molecular Orbital
IPA	Isopropyl Alcohol
IRF	Instrument Response Function
LUMO	Lowest Unoccupied Molecular Orbital
NPL	Nanoplatelet
NVG	Night Vision Goggles

PL	Photoluminescence
PVT	Polyvinyl Toluene
QE	Quantum Efficiency
QIS	Quantum Information Science
SNL	Sandia National Laboratory
TEM	Transmission Electron Microscope
UV	Ultra Violet